Heliyon

ELSEVIER

Received:
29 May 2018
Revised:
24 September 2018
Accepted:
29 November 2018

Cite as: A. Ramesh, P. Tamizhdurai, S. Gopinath, K. Sureshkumar, E. Murugan, K. Shanthi. Facile synthesis of core-shell nanocomposites Au catalysts towards abatement of environmental pollutant Rhodamine B.
Heliyon 5 (2019) e01005.
doi: 10.1016/j.heliyon.2018.e01005

Facile synthesis of core-shell nanocomposites Au catalysts towards abatement of environmental pollutant Rhodamine B

A. Ramesh [a,b], **P. Tamizhdurai** [a], **S. Gopinath** [a], **K. Sureshkumar** [c], **E. Murugan** [b,**], **K. Shanthi** [a,*]

[a] *Department of Chemistry, Anna University, Chennai 600 025, Tamilnadu, India*

[b] *Department of Physical Chemistry, University of Madras, Chennai 600 025 Tamilnadu, India*

[c] *Department of Nanotechnology, Anna University Regional Campus, Coimbatore 641 046, Tamilnadu, India*

[*] Corresponding author.

[**] Corresponding author.

E-mail addresses: dr.e.murugan@unom.ac.in (E. Murugan), kshanthiramesh@yahoo.com (K. Shanthi).

Abstract

Magnetically recoverable Au nanoparticles immobilized/stabilized on core-shell nanocomposites are synthesized by the combination of suspension polymerization as well as surface initiator atom transfer radical polymerization (SI-ATRP) methods. The magnetic core-shell supported Au nanocatalysts are namely Fe_3O_4-PAC-AuNPs, Fe_3O_4-PVBC-g-PAC-AuNPs, Fe_3O_4-HEA-AuNPs, and Fe_3O_4-PVBC-g-HEA-AuNPs. Among all the catalysts, Fe_3O_4-PVBC-g-PAC-Au NPs exhibited an excellent activity in the reduction of Rhodamine B with an apparent rate constant of 10.77×10^{-3} s^{-1} and TOF value of 47.62×10^{-3} s^{-1} under pseudo-first order reaction condition. Further, Fe_3O_4-PVBC-g-PAC-Au NPs has an outstanding activity and recyclability without applying any external magnetic field. This new approach provides an exciting potential way in the preparation of recyclable metal nano-catalysts with high catalytic activity.

Keywords: Materials science, Physical chemistry

https://doi.org/10.1016/j.heliyon.2018.e01005
2405-8440/© 2018 Published by Elsevier Ltd. This is an open access article under the CC BY-NC-ND license (http://creativecommons.org/licenses/by-nc-nd/4.0/).

1. Introduction

In past decades, the development of magnetic recoverable metal based nanocomposites have attracted much interest, because of their critical applications in the field of nanoscience and nanotechnology. It has a broad range of application in electronics, information technology, catalysis, sensor development and biomedical sciences [1, 2]. Apart from that, the metal nanoparticles have large surface area to volume ratio [3, 4]. Interestingly, the wet chemical synthesis routes for magnetic nanoparticles are simple and yields specific shape & size. There are few reports are available regarding the core-shell models. The nanocomposites depends upon the nature of metal oxides used as a core such as SiO_2, Au, TiO_2, Al_2O_3 and the shell may be both organic and inorganic materials [5, 6, 7, 8]. Yu et al., reported dumbbell-like Au-Fe_3O_4 nanoparticles with some drawbacks such as metal leaching, oxidation, and aggregation [9]. To overcome these limitations, magnetic core nanoparticles are often coated with some inert shells such as linear or branched polymer. The polymeric shell coated metal nanoparticles (MNPs) have wide range of applications which includes magnetic targeted drug delivery, contrast enhancement in magnetic resonance imaging (MRI), purification (or) separation of biomolecular agents, catalytic applications, and shape-memory applications [10, 11, 12, 13, 14]. Earlier literature reviews expose the copious amount of work has been done on the generation of shell on the core. Therefore, the desired functional group was introduced onto the magnetic core-shell through surface-initiator atom transfer radical polymerization (SI-ATRP) method. The SI-ATRP is a versatile method which offers several advantages over other polymerization techniques. Furthermore, some ATRP method has been reported to make core-shell system like SiO_2, Au, $MnFe_2O_4$, Au@SiO_2, and Fe_2O_3 [15, 16, 17, 18, 19]. Among different methods, SI-ATRP techniques involve the use of polymer network grafted onto the core was reported [20]. This organic/polymer can offer, inert, reusable, non-toxic, and flexible core-shell catalysts [21, 22, 23]. The surface group consists of both organic and inorganic shells with enhanced physical properties. However, the core-shell nanocomposites have improved catalytic activity in both organic and aqueous medium [24].

Fan et al. [25] reported the polymer shell acts as a good stabilizing agent via ATRP method. Lei et al. [26] also reported the grafting of polymer over the core and also the surface modified Fe_3O_4/SiO_xNPs with high specific surface area. Further, the functionalization and the size of metal particles can be achieved easily. The stabilization of Ag nanoparticles using polyelectrolyte and poly ethylene glycol by layer assembly prevents aggregation and increases the monodispersity [27]. However, these types of homogeneous polyelectrolyte stabilized metal nanoparticles catalysts suffer with some recoverability problem in aqueous/organic phase reaction [24]. Therefore, these types of polymer stabilized metal nanoparticles are coated with

https://doi.org/10.1016/j.heliyon.2018.e01005
2405-8440/© 2018 Published by Elsevier Ltd. This is an open access article under the CC BY-NC-ND license (http://creativecommons.org/licenses/by-nc-nd/4.0/).

insoluble heterogeneous support materials such as a polymer, Fe_3O_4, SiO_2, and Al_2O_3 [20, 23]. Especially, the magnetic core-shell supported materials are effective, eco-friendly and easy to handle. Bulk Au has been found to be inactive whereas, gold nanoparticles (Au NPs) proved to be a highly efficient catalyst [28, 29, 30, 31]. In the photocatalytic degradation of dyes using Au NPs have shown significant selectivity and high activity due to high surface area to volume ratio. Even though unsupported Au NPs have high catalytic activity they tends to aggregate which results in reduced catalytic activity [20]. Au NPs have difficulty in recycling from various catalytic environments. To overcome these problems, the heterogeneous metal nanoparticles in nanometer (nm) range have been immobilized on suitable supports such as carbon, metal oxides, and zeolites [32, 33, 34, 35, 36].

The industrial discharged materials from the food, coloring, cosmetic, paper, textiles and carpet industries are the main sources for aromatic dyes [37]. These aromatic dyes are more stable and difficult to degrade [38]. Moreover; some of the benzidine-based dyes are toxic, carcinogenic and also causes rapid decrease in the amount of dissolved oxygen affecting aquatic life species [39, 40]. Therefore, removal of these dyes from the wastewater before discharge is of greater concern. The removal of color from wastewater can be done via several methods namely chemical, biological and physical methods [41]. Despite the development of various methods for dye degradation each suffers from major drawbacks such as the physical methods have a limited lifetime, the biological method produced toxicity and the chemical method is highly active, but expensive. Therefore to circumvent this problem, there is a need to develop environment friendly, less time consuming and low-cost materials.

The present work, mainly focus on the synthesis of highly stable Au NPs. The synthesis involves suspension polymerization (SP) method which is not able to complete polymerization because of less number of polymers and supported Au NPs (active sites) on the surface of the core. However, this method was combined with SI-ATRP method to develop materials with high stability and reusability. High stable Au NPs catalysts on the surface of Fe_3O_4 were synthesized by the combined synthesis methods. Further, these catalysts are expected to be a potential candidate for the degradation of dyes present in industrial effluents.

2. Materials and methods

2.1. Materials

Ferric chloride hexahydrate (Loba Chemie), ferrous sulphate heptahydrate (SRL), aqueous ammonia (SRL), oleic acid (Merck), divinyl benzene (Sigma-Aldrich), styrene (Sigma-Aldrich), benzoyl peroxide (Alfa Aeser), 2-acryloxyethyltrimethylammonium chloride (Sigma-Aldrich), 2-hydroxyethylacrylate (Sigma-Aldrich), liquid ammonia

https://doi.org/10.1016/j.heliyon.2018.e01005
2405-8440/© 2018 Published by Elsevier Ltd. This is an open access article under the CC BY-NC-ND license (http://creativecommons.org/licenses/by-nc-nd/4.0/).

(SRL), chloroauric acid (Sigma-Aldrich), copper bromide (Sigma-Aldrich), polyethylene glycol (PEG (M.wt-4000)) (SRL), 1,10 phenanthroline (Sd-fine), EDTA (SRL), chloroauric acid (Sigma Aldrich), rhodamine-B (Sigma-Alrich) and sodium borohydride (SRL) were used as such. All the chemicals were of analytical grade with >90% purity. Solvents like methanol (SRL), acetone (SRL), ethanol (SRL), diethylether (SRL), dichloromethane (SRL) and DD water were also used.

2.2. Syntheses of magnetic core-shell based nanocomposite catalysts

2.2.1. Synthesis of core-shell nanocomposites

Fe_3O_4 magnetic particles were prepared via co-precipitation method according to the previous report [42] (Fig. 1). Synthesis of Fe_3O_4-PAC and Fe_3O_4-HEA core-shell nanocomposites were carried out by suspension polymerization technique. Initially, 1 gram (g) of Fe_3O_4-OANPs was dispersed in 40 ml of ethanol. About 2 g of PEG-4000 was dissolved in 100 mL of hot water followed by the addition of 1 mL of styrene (St) (8.7×10^{-3} mol) and 1 ml of divinyl benzene (DVB) (7.2×10^{-2} mol). Then, two different functional monomers such as 2-acryloyloxyethyltrimethylammonium chloride (PAC) (2.33×10^{-2} mol) 4 mL and 2-hydroxyethyl acrylate (HEA) (3.7×10^{-2} mol) of 4 mL were added. The whole reaction mixture was added to the above Fe_3O_4-OA NPs with continuous stirring. Finally, 0.2 g of benzoyl peroxide (BPO) (8.0×10^{-3} mol) dissolved in ethanol was also added dropwise under continuous stirring and heated at 80 degree Celsius (°C) for 4. Finally, Fe_3O_4-PAC NPs and Fe_3O_4-HEA NPs matrix was synthesized Fe_3O_4- poly (vinyl benzyl chloride) (PVBC) magnetic core-shell based materials were synthesized by suspension polymerization techniques (Fig. 1). 1 g of

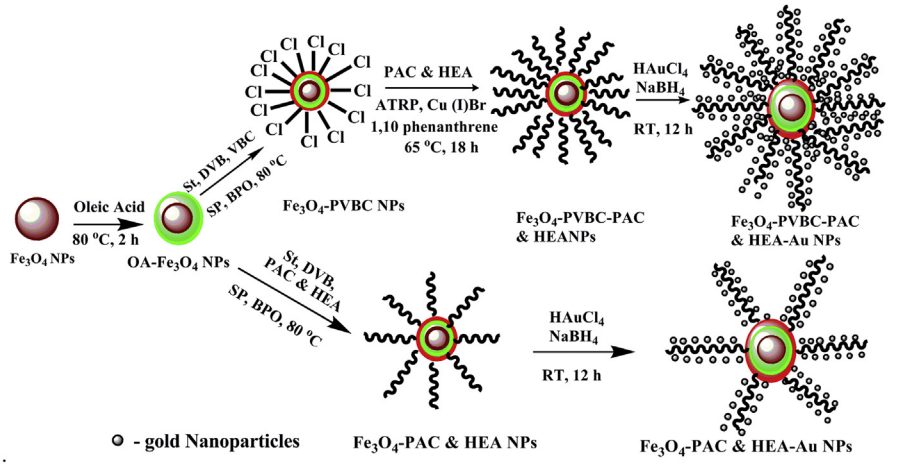

Fig. 1. Synthesis of Fe_3O_4-PAC & HEA-Au NPs and Fe_3O_4-PVBC-g-PAC & HEA-AuNPs magnetic core-shell based nanocomposite catalysts.

https://doi.org/10.1016/j.heliyon.2018.e01005
2405-8440/© 2018 Published by Elsevier Ltd. This is an open access article under the CC BY-NC-ND license (http://creativecommons.org/licenses/by-nc-nd/4.0/).

Fe_3O_4-OANPs was dispersed in ethanol (40 mL) and 2 g of PEG-4000 was dissolved in 100 mL water followed by the addition of 1 mL of styrene (St) (1.1×10^{-2} mol), 1 mL of divinyl benzene (DVB) (7.2×10^{-2} mol) and 4 mL of (2.84×10^{-2} mol) vinyl benzyl chloride (VBC). After, the whole reaction mixture was added to the above Fe_3O_4-OA magnetic fluid solution. Finally, 0.2 g of (8.0×10^{-3} mol) of benzyl peroxide (BPO) was dissolved in 20 mL ethanol and added dropwise, and then the mixture was dried under vacuum at 60 °C for 24 h (Fig. 1).

2.2.2. Grafting of PAC and HEA onto the Fe_3O_4-PVBC matrix by the SI-ATRP

The PAC & HEA were grafted individually onto the Fe_3O_4-PVBC matrix by SI-ATRP technique. 1 g of Fe_3O_4-PVBC matrix in two different RB flasks were dispersed in 50 mL of ethanol, after which 4 mL of PAC (2.33×10^{-2} mol) and HEA (3.7×10^{-2} mol) monomers were added to the respective reaction mixture. After, the calculated amount of Cu (I)Br and 1, 10-phenanthrene were added to the respective reaction mixture and maintained inert atmosphere at 90 °C for 18 h. Then the resulting reaction mixture was filtered followed by the addition of EDTA (10% (w/v)) solution. The reaction mixture was stirred well at RT for 24 h. The resulting Fe_3O_4-PVBC-g-PAC & HEA was filtered and washed followed by dried at 60 °C for 24 h. The obtained product was named as Fe_3O_4-PVBC-g-PAC and Fe_3O_4-PVBC-g-HEA.

2.2.3. Synthesizes of core-shell Au NPs catalysts

Magnetic core-shell supported Au nanoparticles catalysts were prepared by four types of matrix viz., Fe_3O_4-PAC, Fe_3O_4-HEA, Fe_3O_4-PVBC-g-PAC, and Fe_3O_4-PVBC-g-HEA. Initially, 0.5 g of Fe_3O_4-PVBC-g-PAC, Fe_3O_4-PVBC-g-HEA, Fe_3O_4-PAC, and Fe_3O_4-HEA were taken individually and dispersed in ethanol (50 mL) under sonication. Then, 10 mL of aqueous solution of $HAuCl_4$ (7.6×10^{-3} mM, 30 mg) was added to the above reaction mixture and stirred for 2 hat RT. The colour change from brown to yellowish brown was observed during the reaction. Then, 10 mL of $NaBH_4$ (1 mL/10 mM) was added slowly to the above reaction mixture for reduction. The colour of the matrix was changed from yellowish brown to dark brownish purple. This colour change indicated the transformation of Au^{3+} to Au^0 and the produced core-shell magnetic nanoparticles catalysts viz., Fe_3O_4-PAC-AuNPs, Fe_3O_4-HEA-AuNPs, Fe_3O_4-PVBC-g-PAC-AuNPs, and Fe_3O_4-PVBC-g-HEA-AuNPs.

The catalytic activity of four types of catalyst viz., Fe_3O_4-PVBC-g-PAC-AuNPs, Fe_3O_4-PAC-AuNPs, Fe_3O_4-HEA-AuNPs, and Fe_3O_4-PVBC-g-HEA-AuNPs was examined individually from the reduction of rhodamine-B (RhB) under pseudo-first order reaction condition (Fig. 13). The reaction was performed in RB flask,

https://doi.org/10.1016/j.heliyon.2018.e01005
2405-8440/© 2018 Published by Elsevier Ltd. This is an open access article under the CC BY-NC-ND license (http://creativecommons.org/licenses/by-nc-nd/4.0/).

under constant stirring and RT. Initially, 25 mL of (1 mM) liquid $NaBH_4$ solution, 25 mL (0.01 mM) of RhB were taken in RB in which DD water was also added. 8 mg of synthesized catalyst was added into the reaction mixture. The progress of reaction was monitored by Ultra-Violet Visible spectroscopy (UV-Vis spectrum) from the absorbance peak at 554 nm. Moreover, the rate constants were calculated using the following formula (1). The reduction of RhB followed pseudo-first-order kinetics [43]. Therefore, the apparent rate constant (k_{app}) can be defined by the following equation,

$$-\frac{dc_{RhB}}{dt} = KappC - RhB \quad (1)$$

Where,

K_{app} is the apparent rate constant (K_{app}), which is related to the concentration of Au NPs with Fe_3O_4-PVBC-g-PAC stabilized nanocomposites catalysts and concentration of RhB. The k_{app} can be found from the slope of the linear plots of $\ln(C_t/C_0)$ versus time. The reaction is linearly proportional to Au NPs with Fe_3O_4-PVBC-g-PAC stabilized nanocomposites catalysts.

The % degradation efficiency determined by the following formula

$$X = C_0 - C/C_0 \times 100\ \% \quad (2)$$

Where, C_0 and C are the solution concentration or absorbance before and after the degradation respectively. The concentrations of RhB were estimated from UV-Vis spectra peak wavelength.

2.3. Instrumentation

Fourier transform Infra-red spectroscopy (FT-IR) analysis was carried out using BRUKER, TENSOR 27 model instrument. The UV-vis spectra measured using Perkin Elmer ($\lambda = 35$) instrument. Cole-Parmer sonication bath was used for ultrasonication of Fe_3O_4 and various functionalized Fe_3O_4 at 40 kilo electron volts KeV. The surface morphology was performed using VEGA3 TESCAN model scanning electron microscope (SEM). The crystallinity of synthesized catalysts was confirmed by X-ray diffractometer using a Cu kλ monochromatic radiation source ($\lambda = 1.54045$ Å). The magnetic susceptibility values were recorded for the prepared magnetic core-shell based nano-composites using Lakeshore model 7404 with high & low-temperature attachments, at the maximum magnetic field of −2.17 T (0.6 air gap). The high-resolution transmission electron microscopy (HR- TEM) measurement was carried out using an FEI TECNAI G2 model T-30. Thermogravimetric analysis (TGA) was performed using Perkin Elmer under nitrogen atmosphere in the temperature range 30−750 °C at heating a rate of 8 °C min^{-1}.

https://doi.org/10.1016/j.heliyon.2018.e01005
2405-8440/© 2018 Published by Elsevier Ltd. This is an open access article under the CC BY-NC-ND license (http://creativecommons.org/licenses/by-nc-nd/4.0/).

2.4. Photo catalytic reactor setup

The catalytic activity of Fe_3O_4-PVBC-g-PAC-AuNPs, Fe_3O_4-PAC-AuNPs, Fe_3O_4-HEA-AuNPs, and Fe_3O_4-PVBC-g-HEA-AuNPs was examined individually by conducting the degradation of RhB as a model reaction kept under identical pseudo-first order reaction condition. The photo catalytic reactor contains borosilicate glass tube with 20 mm diameter, 40 cm height and 50 milliliter (mL) reaction vessel. The reaction mixture was magnetically stirred for 30 min to maintain adsorption−desorption equilibrium between the dyes and catalysts under constant stirring and ambient temperature by the use of water circulating pump. Exactly, 25 mL of (1 mM) $NaBH_4$ solution, 25 mL (0.01 mM) of aqueous RhB were taken with DD water. 8 milligram (mg) of catalyst was added into the reaction mixture. The sample was first analyzed in the dark (without using light). A 500 W tungsten lamp was used as a visible-light source distanced 6 cm from the reactor vessel. The radiation from the light source was found to be in the visible region at a wavelength of 410 nm. In presence of light, 3 mL of aliquot was withdrawn at regular time interval of 3 min and separated the catalyst using an external magnetic field. The extent of degradation was monitored using Ultraviolet-visible (UV-Vis) spectrophotometer.

3. Results and discussion

3.1. Crystallite analysis

The synthesized catalysts were analyzed by X-Ray diffraction (XRD) to find the crystallinity of Fe_3O_4NPs, Fe_3O_4-OA NPs, Fe_3O_4-PVBC NPs, Fe_3O_4-PVBC-g-PACNPs, and Fe_3O_4-PVBC-g-PAC-AuNPs (Fig. 2a−e). According to Joint committee powder diffraction standard (JCPDS) database (JCPDS No: 19-0629), the XRD pattern of Fe_3O_4 NPs (Fig. 2a) was confirmed from five strong diffraction peaks at a 2Θ values of 30.33°, 35.60°, 43.39°, 57.2° and 62.9° corresponding to (220), (311), (400), (422), and (511) planes respectively. Using the Debye-Scherer equation, the particle size of Fe_3O_4 NPs was calculated to be 12.2 nm from (311) reflection. The XRD patterns of bare Fe_3O_4NPs and Fe_3O_4-OA NPs, Fe_3O_4-PVBC NPs and Fe_3O_4-PVBC-g-PAC NPs are shown in Fig. 2a−e respectively. This suggests that irrespective of magnetic core, the peak intensity of five strong characteristic peaks noticed in bare-Fe_3O_4NPs at 2Θ values of 30.33°, 35.60°, 43.39°, 57.2° and 62.9° were found to decreased in the intensity. This is due to the grafting of −OA, PVBC & PAC. From the Debye-Scherer equation, it has been observed that the size of magnetic Fe_3O_4-OANPs was found to be 14.3 nm. For Fe_3O_4-PVBC NPs and Fe_3O_4-PVBC-g-PAC NPs, the particle size was found to be 17.87 nm 20.17 nm respectively. Increased size of magnetic core-shell is due to the intense grafting of polymers supports, which has been observed from −OA < PVBC < PAC order. Besides these peaks, after the stabilisation/immobilization of Au onto the respective

https://doi.org/10.1016/j.heliyon.2018.e01005
2405-8440/© 2018 Published by Elsevier Ltd. This is an open access article under the CC BY-NC-ND license (http://creativecommons.org/licenses/by-nc-nd/4.0/).

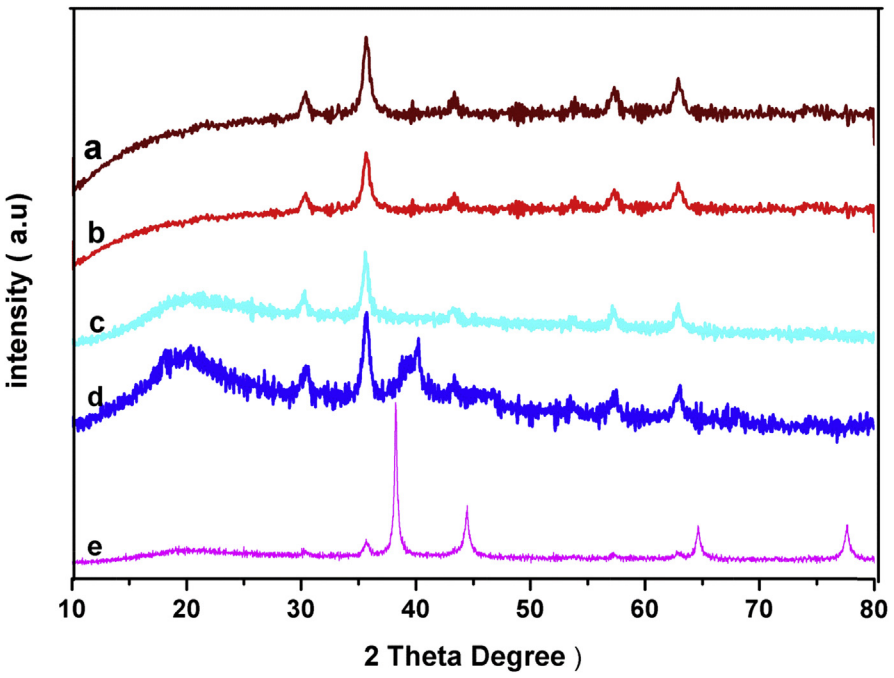

Fig. 2. High angle XRD pattern of (a) Fe_3O_4 NPs, (b) Fe_3O_4-OANPs, (c) Fe_3O_4-PVBC NPs, (d) Fe_3O_4 −PVBC-g-PACNPs and (e) Fe_3O_4−PVBC-g-PAC-AuNPs catalysts.

magnetic matrix, appearance of new peaks at 2Θ values of 38.28° and 44.45° are observed. Other diffraction planes are completely diminished which confirms the existence of AuNPs immobilised on the respective magnetic core-shell. From the XRD plane, the average nanoparticles size of AuNPs was calculated to be 26.65 nm.

3.2. FT-IR analysis

Oleic acid (OA) was coated onto the Fe_3O_4 NPs to prevent the aggregation of the particles. The obtained products viz., Fe_3O_4 & Fe_3O_4-OA NPs was characterised by FT-IR and the respective spectra are shown in Fig. 3a and b respectively. The characteristic peak at 585 cm^{-1} due to Fe-O bond suggests the formation of magnetic Fe_3O_4 NPs. Fe_3O_4-OA NPs (Fig. 3b) shows the characteristic peaks at 1413, 1675, 2844 and 3411 cm^{-1} corresponding to C=C, C=O, $-CH_3$, $-CH_2$ and OH group respectively. These results may be due to the presence of OA on the surface of magnetic Fe_3O_4 NPs.

The obtained Fe_3O_4-OANPs was used as a core moiety on which two different types of poly(styrene) was grafted through suspension polymerization techniques using styrene (supporting monomer), DVB (cross-linking agent), followed by the addition of PAC (functional monomer). The core-shell matrices Fe_3O_4-PACNPs and the respective FTIR spectrum is shown in Fig. 2c. Fig. 3c shows the characteristic peaks at 1624 and 1113 cm^{-1} due to the functionalization of PAC onto the surface of

https://doi.org/10.1016/j.heliyon.2018.e01005
2405-8440/© 2018 Published by Elsevier Ltd. This is an open access article under the CC BY-NC-ND license (http://creativecommons.org/licenses/by-nc-nd/4.0/).

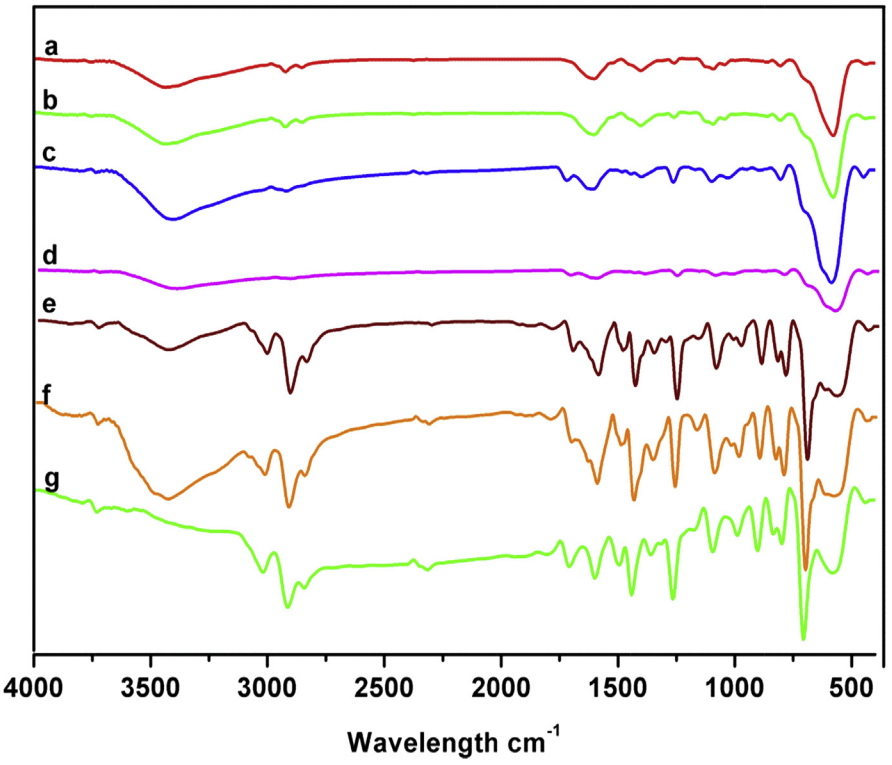

Fig. 3. FT-IR spectrum of (a) Fe_3O_4 (b) Fe_3O_4.OANPs, (c) Fe_3O_4-PAC-NPs, (d) Fe_3O_4—PAC AuNPs, (e) Fe_3O_4-PVBC NPs, (f) Fe_3O_4—PVBC-g-PACNPs and (g) Fe_3O_4—PVBC-g-PAC-AuNPs.

Fe_3O_4-OANPs. However, in the corresponding Fe_3O_4—PAC-AuNPs catalysts, the C-N stretching peak noticed at 1113 cm^{-1} in Fe_3O_4—PAC-AuNPs catalysts were shifted to 1123 cm^{-1}, which confirmed the immobilisation of AuNPs on Fe_3O_4—PACNPs as shown in Fig. 3d.

Further, poly (vinyl benzyl chloride) was functionalized on Fe_3O_4-OANPs core via suspension polymerization and named as Fe_3O_4-PVBC NPs. This product was characterised by FTIR and is shown in Fig. 3e. The peaks noticed at 705 and 1485 cm^{-1} region due to C-Cl and -CH_2 stretching vibration respectively. This confirms the functionalization of poly (vinyl benzyl chloride) on to the Fe_3O_4-OANPs. Then using this Fe_3O_4-PVBC NPs as a common matrix, the PAC was grafted (g) through the SI-ATRP method and named as Fe_3O_4-PVBC-g-PACNPs. The corresponding FTIR spectra for these matrices are shown in Fig. 3f. The Fe_3O_4-PVBC-g-PAC NPs characteristic peaks were observed for aromatic C-H vibration at 3027 cm^{-1}, aliphatic C-H stretching vibration at 2920 cm^{-1}, CH_2 bending vibration at 1438 cm^{-1} and appearance of these peaks evidences the successful grafting of PAC onto the Fe_3O_4-PVBC matrix. The Fig. 3f shows the FTIR spectrum of Fe_3O_4-PVBC-g-PAC NPs and the characteristic peaks at 1701 & 1148 cm^{-1} are due to C=O & C-N stretching vibrations respectively. This confirms that PAC was grafted on the Fe_3O_4-PVBC NPs. Moreover, The FTIR spectra of Fe_3O_4—PVBC-g-PAC-Au

https://doi.org/10.1016/j.heliyon.2018.e01005
2405-8440/© 2018 Published by Elsevier Ltd. This is an open access article under the CC BY-NC-ND license (http://creativecommons.org/licenses/by-nc-nd/4.0/).

NPs catalysts were shown in Fig. 3g. The C-N stretching peak noticed at 1148 cm^{-1} in Fe_3O_4−PAC-AuNPs catalysts shifted to 1154 cm^{-1}, which confirms the presence of Fe_3O_4-PVBC-PAC-AuNPs.

3.3. UV-visible spectrum

From, Fig. 4, the UV-vis-spectra of (a) Fe_3O_4-PAC-AuNPs and (b) Fe_3O_4-PVBC-g-PAC-AuNPs is observed. The catalysts were dispersed individually in ethanol, and the metal nanoparticles were extracted irrespective of the catalyst to establish the stabilisation/immobilisation of AuNPs onto Fe_3O_4-PACNPs and Fe_3O_4-PVBC-g-PACNPs. All these extracted catalytic solutions contain AuNPs and analysed with UV- Vis spectroscopy regardless of the catalysts solution. The surface plasmon resonance (SPR) peaks present at 531 nm confirms the formation of AuNPs catalysts onto the surface of Fe_3O_4-PACNPs and Fe_3O_4-PVBC-g-PAC NPs.

3.4. Vibrating sample magnetometer (VSM) analysis

The VSM spectra analysis was performed to observe the magnetic properties of Fe_3O_4 NPs, (b) Fe_3O_4-OA NPs, (c) Fe_3O_4-PAC-AuNPs, and (d) Fe_3O_4-PVBC-g-PAC-AuNPs at RT and the corresponding VSM spectra are shown in Fig. 5. The M-H sigmoidal curve for the core-shell Fe_3O_4-polymer nano-composite catalysts are shown in Fig. 5a−d. The saturation magnetisation values (Ms) for Fe_3O_4NPs, Fe_3O_4-OANPs, Fe_3O_4-PAC-AuNPs, and Fe_3O_4-PVBC-g-PAC-AuNPs was found

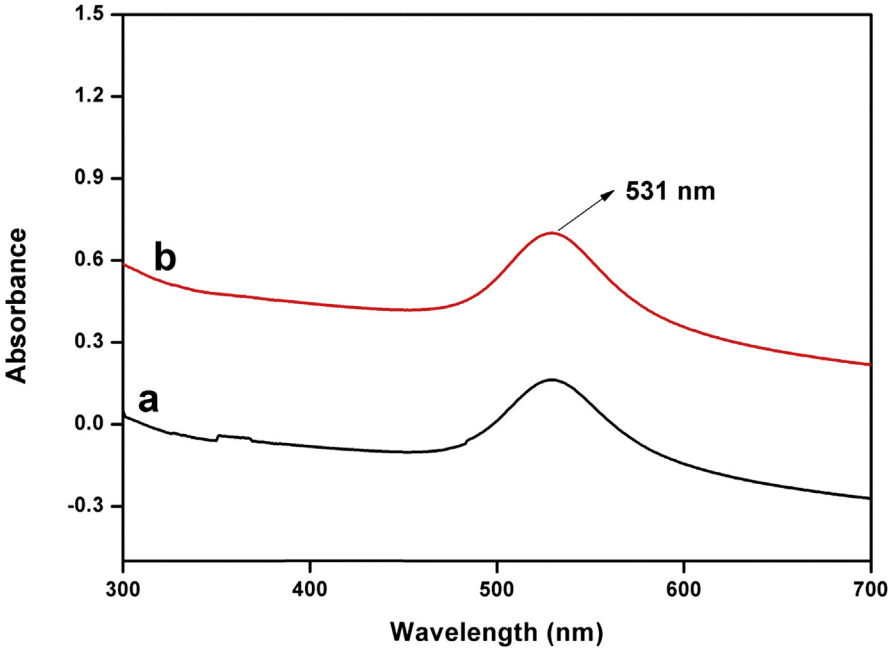

Fig. 4. UV-Vis Spectrum of a) Fe_3O_4-PAC-AuNPs and b) Fe_3O_4-PVBC-g-PAC-AuNPs.

https://doi.org/10.1016/j.heliyon.2018.e01005
2405-8440/© 2018 Published by Elsevier Ltd. This is an open access article under the CC BY-NC-ND license (http://creativecommons.org/licenses/by-nc-nd/4.0/).

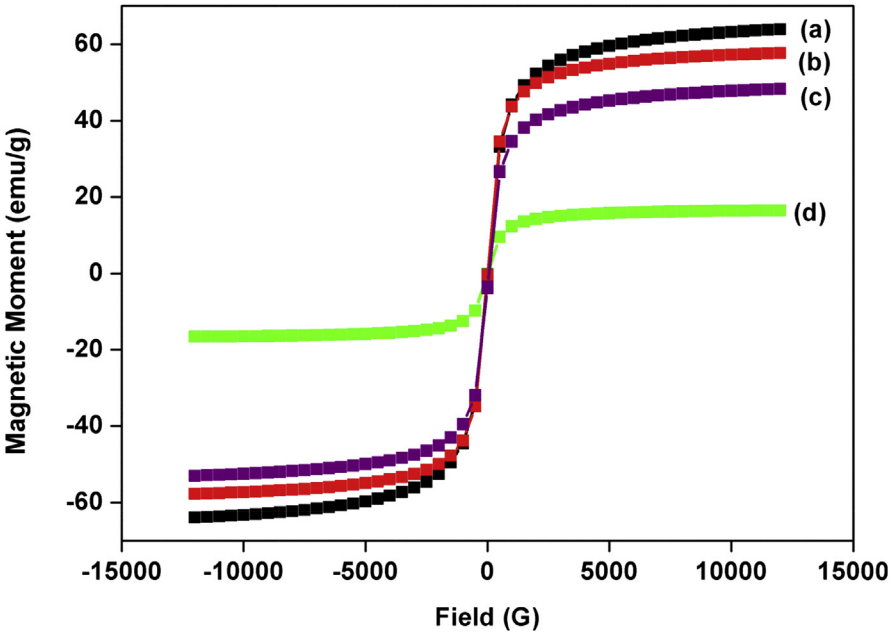

Fig. 5. VSM spectra of (a) Fe_3O_4 NPs (b) Fe_3O_4-OA NPs, (c), Fe_3O_4-PAC-AuNPs (d) Fe_3O_4—PVBC-g-PAC-AuNPs catalysts.

to be 63.89, 57.58, 47.98 and 16.50 emu/g respectively. This observation undoubtedly indicates that all these composites exhibited superparamagnetic behavior. When PAC was grafted onto the PVBC and coated on Fe_3O_4NPs via SI-ATRP technique, the Ms values have been decreased. The corresponding VSM spectra were shown in Fig. 5a—d. The decreased Ms value of matrix derived from SI-ATRP method Fe_3O_4-PVBC-g-PAC-AuNPs has shown lower Ms value around 16.50 emu/g due to more number of functional group grafted onto the surface. However, the suspension method has higher Ms value (47.98 emu/g) due to less number of functional group onto the surface of Fe_3O_4 NPs.

3.5. TGA analysis

Thermogravimetric analysis (TGA) was measured to observe any changes in physical and chemical properties as a function of temperature. Fig. 6a—c shows TGA curves of (a) Fe_3O_4 NPS, (b) Fe_3O_4-PAC-AuNPs and (c) Fe_3O_4-PVBC-g-PAC-AuNPs, which confirms the weight change during polymerization. Fe_3O_4NPs exhibited the loss of about only 3% up to 750°C was recorded. This might be due to the evaporation of physisorbed water molecules on the surface, and no other weight losses have been observed during the reaction. From Fig. 6b and c it has been observed a weight loss upto 490 °C was recorded for core-shell Fe_3O_4-PAC-AuNPs and Fe_3O_4-PVBC-g-PAC-AuNPs.

The major weight loss of Fe_3O_4-PAC AuNPs and Fe_3O_4-PVBC-g-PAC-AuNPs observed at 210 °C—410 °C, respectively. The core-shell Fe_3O_4-PAC-AuNPs has

https://doi.org/10.1016/j.heliyon.2018.e01005
2405-8440/© 2018 Published by Elsevier Ltd. This is an open access article under the CC BY-NC-ND license (http://creativecommons.org/licenses/by-nc-nd/4.0/).

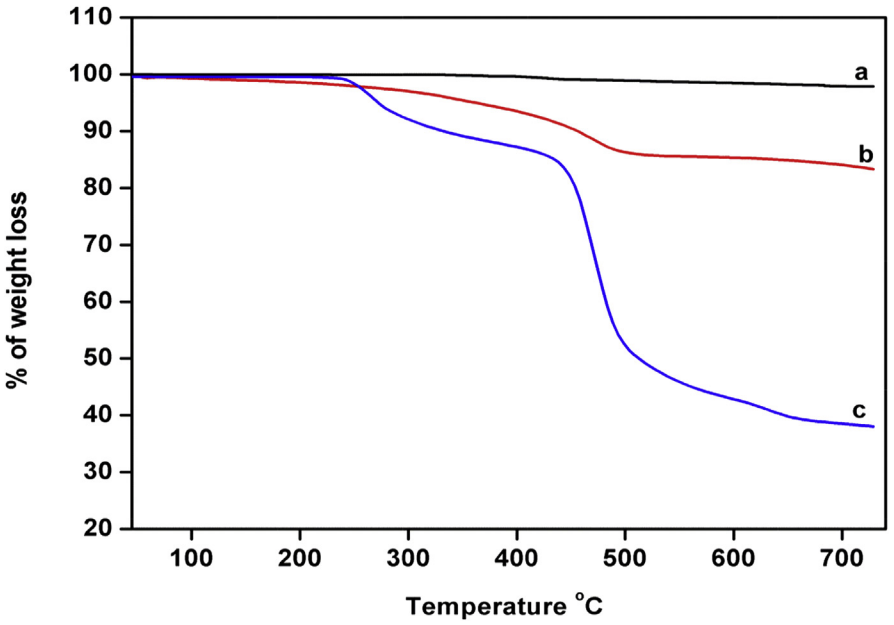

Fig. 6. TGA analysis of a) Fe_3O_4NPs, b) Fe_3O_4-PAC-AuNPs and c)Fe_3O_4−PVBC-g-PAC-AuNPs.

42 % weight loss that is due to the small amount of polymer shell was coated onto the surface of Fe_3O_4 NPs. Fe_3O_4-PVBC-g-PAC-AuNPs has 60 % weight loss due to SI-ATRP grafting methods. From Fig. 6c the magnetic core-shell nanocomposite catalyst has two weight loss, the first weight loss of 26 % at 200 °C which is attributed to the loss of surface moieties and the second weight loss of 34% at 405 °C indicating the growth of the polymers on the surface of Fe_3O_4 NPs were observed. Hence, the TGA results reveal that the SI-ATRP method is superior than the suspension method.

3.6. TEM and SEM analysis

TEM and SEM analysis were carried out for Fe_3O_4-PAC-AuNPs, Fe_3O_4-HEA-AuNPs, Fe_3O_4-PVBC-g-PAC-AuNPs and Fe_3O_4-PVBC-g-HEA-AuNPs. Based on the results, the catalysts obtained from PAC and PVBC-g-PAC has been proved to be the best catalyst than the rest of the catalysts. Fig. 7a and b shows the TEM images of Fe_3O_4−PVBC-g-PAC-AuNPs and Fig. 7c and d shows the SEM images of Fe_3O_4−PVBC-g-PAC-AuNPs.

The TEM image of Fe_3O_4−PVBC-g-PAC-AuNPs confirms the spherical morphology. However, the spherical core-shell with intense black dots suggests that AuNPs are well dispersed over the core-shell nanocomposites with an average size of 26.65 nm. Two set of NPs were measured with an average particle size of 6.6 nm Au NPs and 26.65 nm. Furthermore, the SEM images also exhibit the same results of spherical morphology. Besides, based on the XRD results, Fe_3O_4−PVBC-g-

https://doi.org/10.1016/j.heliyon.2018.e01005
2405-8440/© 2018 Published by Elsevier Ltd. This is an open access article under the CC BY-NC-ND license (http://creativecommons.org/licenses/by-nc-nd/4.0/).

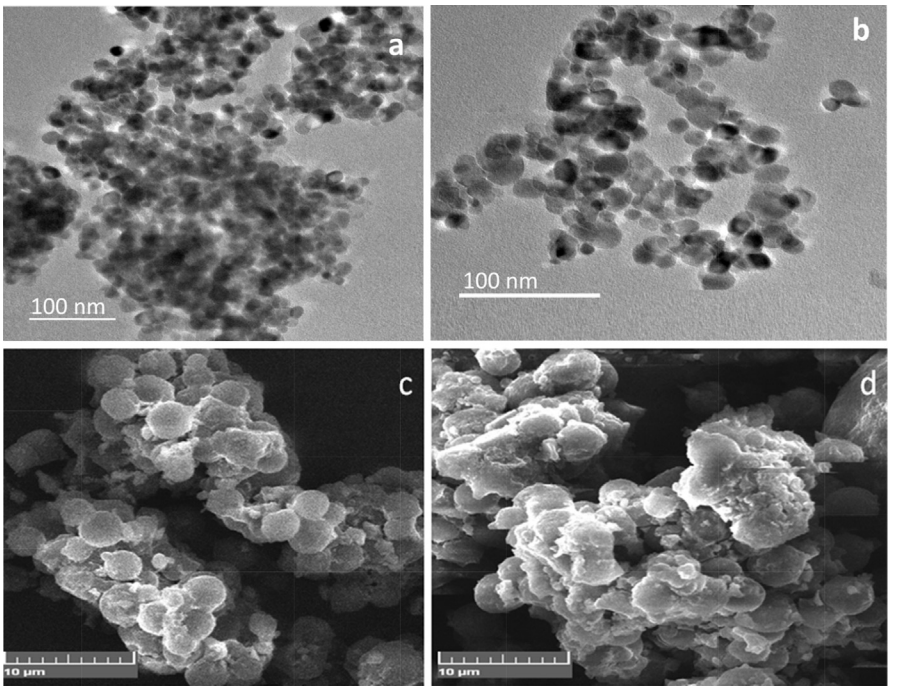

Fig. 7. TEM images of (a) & (b) Fe_3O_4−PVBC-g-PAC-Au NPs and SEM images (c) & (d) Fe_3O_4−PVBC-g-PAC-AuNPs catalyst.

PAC-AuNPs exhibited the sharp intensity peak which confirms the formation of nanomaterials. Moreover, the SEM images show the intense white dots and patches in Fe_3O_4-PVBC-g-PAC-AuNPs catalysts, which conforms more amount of loading (or) stabilisation of Au NPs. This results confirms SI-ATRP modified Fe_3O_4-PVBC-g-PAC- AuNPs matrix contains more N-C functional group than the rest of the matrix.

4. Analysis

4.1. Comparative catalytic activity

The catalytic activities of Fe_3O_4-PAC-Au NPs, Fe_3O_4-HEA-Au NPs, Fe_3O_4-PVBC-g-PAC-Au NPs, and Fe_3O_4-PVBC-g-HEA-AuNPs catalysts were examined in the reduction of RhB dye. The reaction was monitored by UV-Vis spectroscopy (Fig. 8). The intensity of the characteristic peak viz., C=N at 554 nm was quantitatively determined at regular time interval of (3 min) and k_{app} was calculated from Eq. (1). The K_{app}, degradation efficiency and TOF were calculated for the reductions of RhB are given in Table 1 (including the correlation co-efficient (R^2) and degradation efficiency %) and Fig. 8a−d. The k_{app}, degradation efficiency was calculated from Eq. (2) and TOF is calculated from Eq. (1) for Fe_3O_4-PAC-AuNPs, Fe_3O_4-HEA-AuNPs, Fe_3O_4-PVBC-g-HEA-AuNPs and Fe_3O_4-PVBC-g-PAC-AuNPs catalysts

https://doi.org/10.1016/j.heliyon.2018.e01005
2405-8440/© 2018 Published by Elsevier Ltd. This is an open access article under the CC BY-NC-ND license (http://creativecommons.org/licenses/by-nc-nd/4.0/).

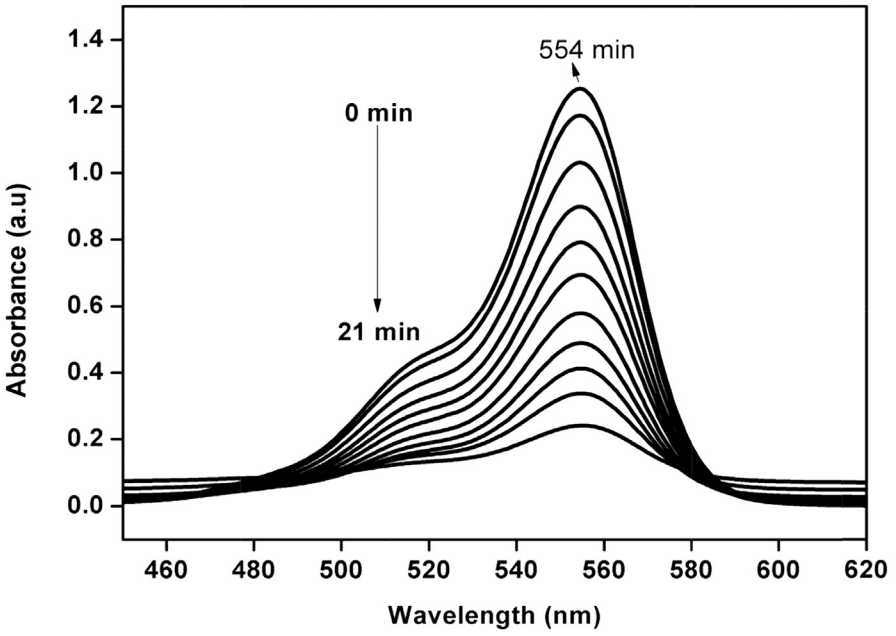

Fig. 8. UV-Vis Spectrum Degradation of RhB using Fe_3O_4-PVBC-g-PAC-AuNPs catalyst.

Table 1. The comparative catalytic activity of four types of MNPs catalysts for apparent rate constant, TOF and the efficiency towards reduction of RhB.

S. No	Name of the catalyst	$K_{app} \times 10^{-2}\ s^{-1}$	$TOF \times 10^{-3}\ s^{-1}$	Degradation efficiency (%)	Correlation co-efficient (R^2)
1	Fe_3O_4-PAC-AuNPs	2.90	1.18	44.23	0.9921
2	Fe_3O_4-HEA-AuNPs	2.44	1.0	29.15	0.9925
3	Fe_3O_4-PVBC-g-HEA-AuNPs	7.74	33.3	85.35	0.9944
4	Fe_3O_4-PVBC-g-PAC-AuNPs	10.77	47.62	99.30	0.9989

are almost same amount. The K_{app} values are $2.90 \times 10^{-2}\ s^{-1}$, $2.44 \times 10^{-2}\ s^{-1}$, $7.74 \times 10^{-2}\ s^{-1}$ and $10.77 \times 10^{-3}\ s^{-1}$ and corresponding TOF values are $1.18 \times 10^{-3}\ s^{-1}$ and $1.0 \times 10^{-3}\ s^{-1}$,$33.3 \times 10^{-3}\ s^{-1}$ and $47.62 \times 10^{-3}\ s^{-1}$ respectively. Among the different catalysts, Fe_3O_4-PVBC-g-PAC-AuNPs was found to be highly active due to the size of the MNPs and more numbers activity sites (functional group) stabilized as compared to the rest of the catalysts (Table 1) and (Fig. 9a–d). The Kapp, TOF and degradation efficiency values of Fe_3O_4-PVBC-g-PAC-Au NPs catalyst synthesized by SI-ATRP method are 10.77×10^{-3} (s^{-1}), 47.62×10^{-3} (s^{-1}) and 99.9%. In general, high loading is possible due to the availability of more C-N^+ (-N^+-(-CH_3)$_3$) groups and thus proportionally stabilised the metal nanoparticles, which in turn reflected an increased catalytic activity in the degradation of RhB reaction. Therefore, this preferred catalyst was chosen for the

https://doi.org/10.1016/j.heliyon.2018.e01005
2405-8440/© 2018 Published by Elsevier Ltd. This is an open access article under the CC BY-NC-ND license (http://creativecommons.org/licenses/by-nc-nd/4.0/).

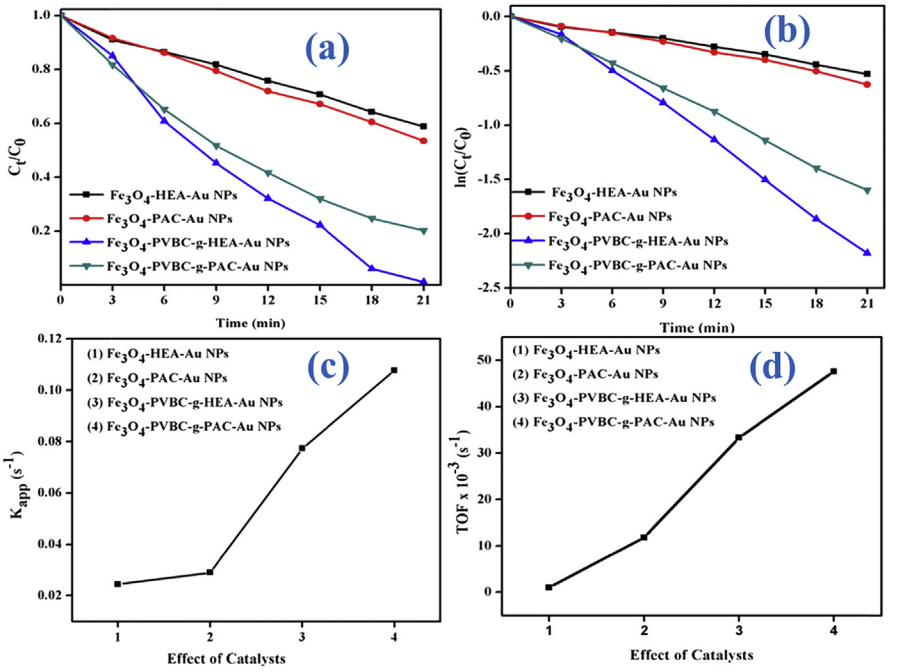

Fig. 9. (a) Normalized absorbance at λmax of RhB vs AuNPs catalysts, C_t is the conc. of RhB at real time '*t*' and C_0 is the conc. of MB. (b) $\ln(C_t/C_0)$ at 554 nm vs. reaction time for the reduction of MB. (c) Figure of apparent rate constant (k_{app}) as function of different catalysts (d) Figure of TOF as function of different catalysts.

kinetic study under the same reaction condition by varying the substrate and the catalyst.

4.2. Effect of catalysts

On increasing the concentration of catalyst viz., Fe_3O_4-PVBC-g-PAC-AuNPs, the K_{app} was found to increase linearly. In the present study, the amount of catalyst has been varied from 2 mg to 10 mg keeping the other parameters as constant. The K_{app} values are 7.70×10^{-2} s^{-1}, 9.0×10^{-2} s^{-1}, 10.77×10^{-2} s^{-1}, 11.89×10^{-2} s^{-1} and 12.85×10^{-3} s^{-1} and corresponding TOF values are 37×10^{-3} (s^{-1}), 41×10^{-3} (s^{-1}), 47×10^{-3} (s^{-1}), 62×10^{-3} (s^{-1}), and 83×10^{-3} (s^{-1}) respectively. Normally, when the substrate concentration is fixed, the catalyst concentration increases the k_{app} and TOF values as shown in Fig. 10a–d and corresponding values are tabulated in Table 2 (including the efficiency %, correlation co-efficient (R^2)).

4.3. Effect of [RhB]

To determine the substrate concentration of RhB in the presence of Fe_3O_4-PVBC-g-PAC-AuNPs catalyst under identical reaction condition, the concentration of

https://doi.org/10.1016/j.heliyon.2018.e01005
2405-8440/© 2018 Published by Elsevier Ltd. This is an open access article under the CC BY-NC-ND license (http://creativecommons.org/licenses/by-nc-nd/4.0/).

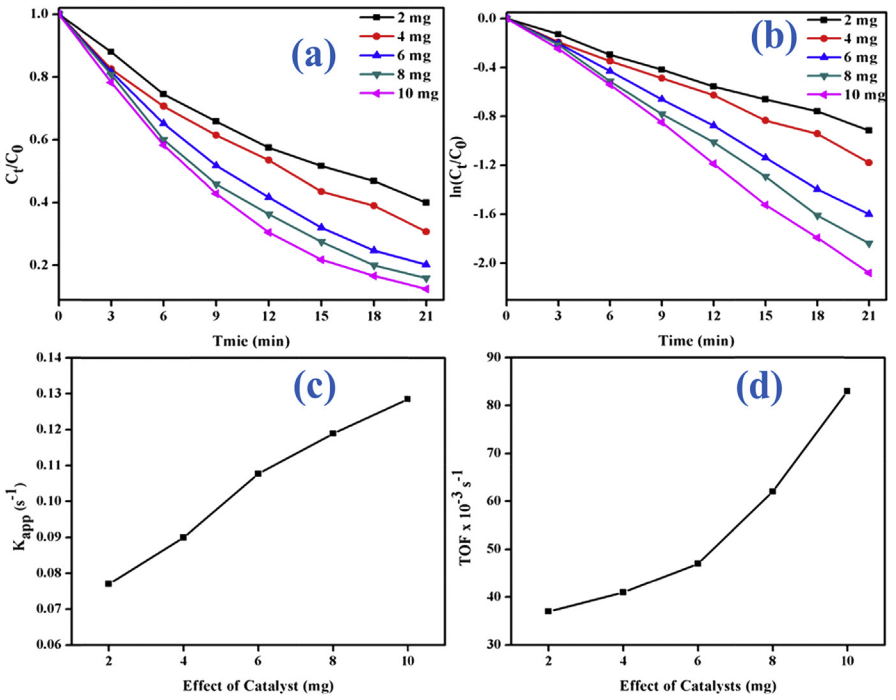

Fig. 10. (a) Normalized absorbance at λ_{max} of RhB VsFe$_3$O$_4$-PVBC-g-PACAuNPs catalysts, C_t is the conc. of RhB at real time t and C_0 is the conc. of RhB. (b) ln(C_t/C_0) at 554 nm vs. reaction time for the reduction of RhB. (c) Figure of apparent rate constant (k_{app}) as function of different catalysts (d) Figure of TOF as function of different catalysts.

substrate was varied from 6×10^{-3} mM to 14×10^{-3} mM. The k_{app} was calculated and plotted against the substrate amount (Fig. 11). Moreover, the corresponding percentages of degradation efficiency values are shown in Table 1.

While increasing the RhB concentration, the concentration of the catalyst remains constant. The active sites on the catalysts are found to be less as the concentration of dye molecules is high. Hence, the catalytic activity was gradually decreased due to less number of active sites. Therefore, Fe$_3$O$_4$-PVBC-g-PAC-AuNPs materials act as a suitable catalyst towards the degradation of RhB [38].

Table 2. Effect of catalysts for apparent rate constant, TOF and the efficiency towards reduction of RhB.

S. No	Fe$_3$O$_4$-PVBC-g-PAC-AuNPs	$K_{app} \times 10^{-2}$ s^{-1}	TOF $\times 10^{-3}$ s^{-1}	Degradation efficiency (%)	Correlation co-efficient (R^2)
1	2.0 mg	7.7	37	90	0.9957
2	4.0 mg	9.0	41	93	0.9961
3	6.0 mg	10.77	47	99	0.9989
4	8.0 mg	11.89	62	99.9	0.9986
5	10.0 mg	12.85	83	99.9	0.9987

https://doi.org/10.1016/j.heliyon.2018.e01005
2405-8440/© 2018 Published by Elsevier Ltd. This is an open access article under the CC BY-NC-ND license (http://creativecommons.org/licenses/by-nc-nd/4.0/).

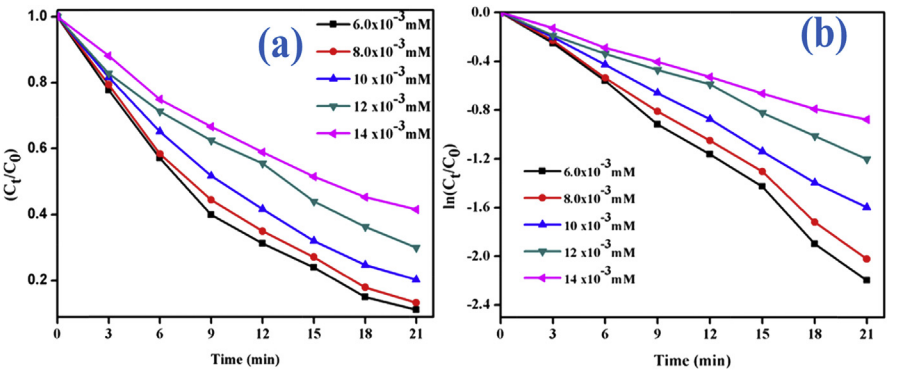

Fig. 11. Effect of [RhB] plots a) concentration of RhB plots C_t/C_0 vs Time (min) and b) concentration of RhB plots $\ln(C_t/C_0)$vs Time (min) by using Fe3O4-PVBC-g-PACAuNPs catalysts.

4.4. Recycle efficiency

Stability and the recyclability of the catalyst are more important for any catalytic reactions. The Fe_3O_4-PVBC-g-PAC-AuNPs catalysts were filtered, dried and reused for the same reaction for which K_{app} value of 8.96×10^{-2} min^{-1} was maintained in the right catalyst. The recycling efficiency of magnetic core-shell based metal nanoparticles catalyst viz., Fe_3O_4-PVBC-g-PAC-AuNPs was examined up to sixth cycle. The obtained rate constant was found to be almost similar, irrespective of the cycle which indicates the sound stability of the catalyst (Fig. 12).

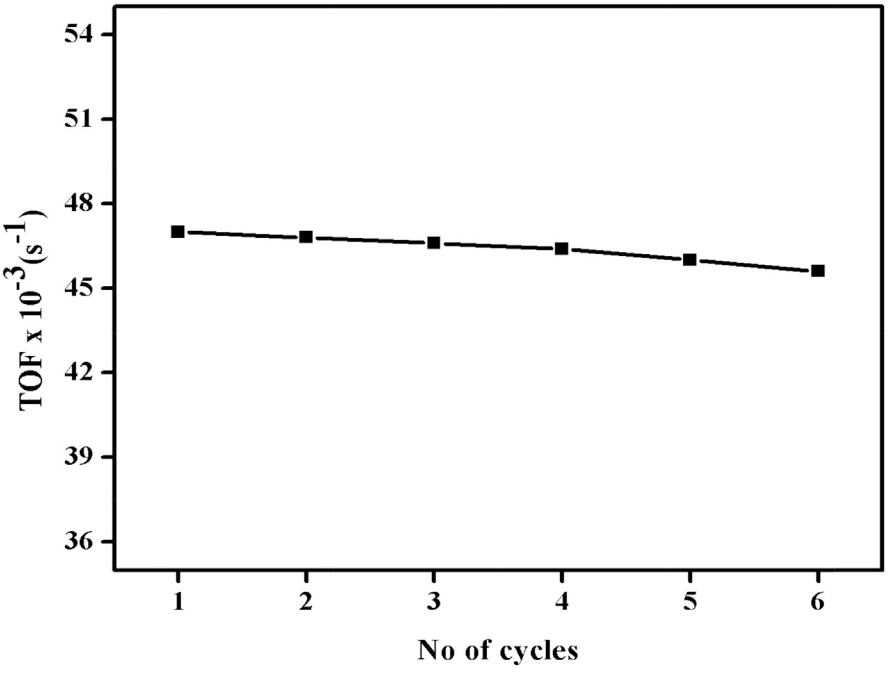

Fig. 12. Re-cycle for superior catalyst viz., Fe_3O_4-PVBC-g-PAC-AuNPs.

https://doi.org/10.1016/j.heliyon.2018.e01005
2405-8440/© 2018 Published by Elsevier Ltd. This is an open access article under the CC BY-NC-ND license (http://creativecommons.org/licenses/by-nc-nd/4.0/).

4.5. Mechanism of RhB degradation

The catalytic activity of catalysts viz., Fe_3O_4-PAC-AuNPs, Fe_3O_4-HEA-AuNPs, Fe_3O_4-PVBC-g-PAC-AuNPs, and Fe_3O_4-PVBC-g-HEA-AuNPs were measured separately by conducting the degradation of Rhodamine B (RhB). The experiment was performed with excess $NaBH_4$ keeping under identical pseudo-first order reaction conditions. It was monitored that the decrease in peak intensity of RhB was noticed at 554 nm which can be clearly shows the reduction take place. The reduction of RhB by these Au NPs catalysts occurred only via the destruction of conjugated structure [34].

A possible catalytic mechanism for the degradation of RhB using magnetic core-shell based nanocomposites catalyst follows an intermediate mechanism. The monomer exhibited a high absorption band at 554 nm in an aqueous medium matches with $n-\pi^*$ transitions. Since BH_4^- can act as an electron donor (nucleophile) while RhB serves as an electrophile concerning Fe_3O_4-PVBC-g-PAC-Au NPs catalyst, the nucleophile BH_4 can offer electrons to Fe_3O_4-PVBC-g-PAC-Au NPs catalyst; Next, the electrophile RhB can receive electrons from the catalyst. Thus, the Fe_3O_4-PVBC-g-PAC-Au NPs catalyst behaves as an electron relay for RhB degradation in a $NaBH_4$ solution. The availability of more number of quaternary ammonium chloride and is possible due to increased complex of Au on Fe_3O_4-PVBC-g-PAC-AuNPs. The increased complex concentration was higher because of greater availability of $-N^+(CH_3)_3$ group on the periphery of Fe_3O_4-PVBC-g-PAC-AuNPs than HEA functional group.

The effective degradation/reduction of RhB was carried out and the reaction condition was optimized. However, this preferred catalyst via, Fe_3O_4-PVBC-g-PAC-AuNPs was employed to determine thorough kinetics, and these catalysts can be used as industrial catalysts with high stability and reusability.

4.6. GC-MS analysis

The catalytic activity of photo degradation of RhB was analysis by GC-MS and as given Fig. 13. The initial concentration of RhB was analyses the retention time of peak position are noted. The photocatalytic reaction was carried out in the presence of Fe_3O_4-PVBC-PAC Au NPs catalysts under the assayed reaction condition. The initial concentration of dye molecule has been various peaks determine with high retention time peaks intensity as shown in Fig. 13a. From Fig. 14b, after reaction take place the peaks positions were shifted the low retention time with less intensity as shown in Fig. 13b. However, the GC-MS results reveal that the low retention time (low concentration of RhB) this may be complete reduction/degradation of RhB.

https://doi.org/10.1016/j.heliyon.2018.e01005
2405-8440/© 2018 Published by Elsevier Ltd. This is an open access article under the CC BY-NC-ND license (http://creativecommons.org/licenses/by-nc-nd/4.0/).

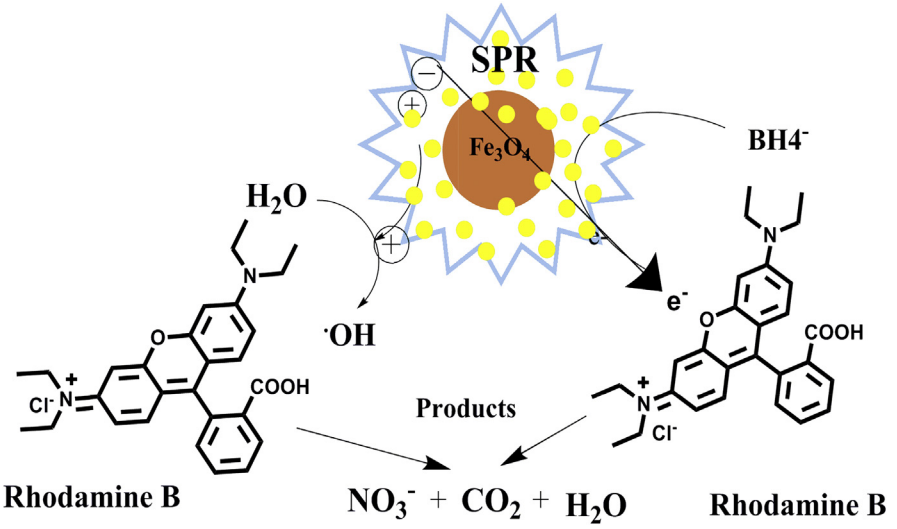

Fig. 13. Mechanism for degradation of RhB.

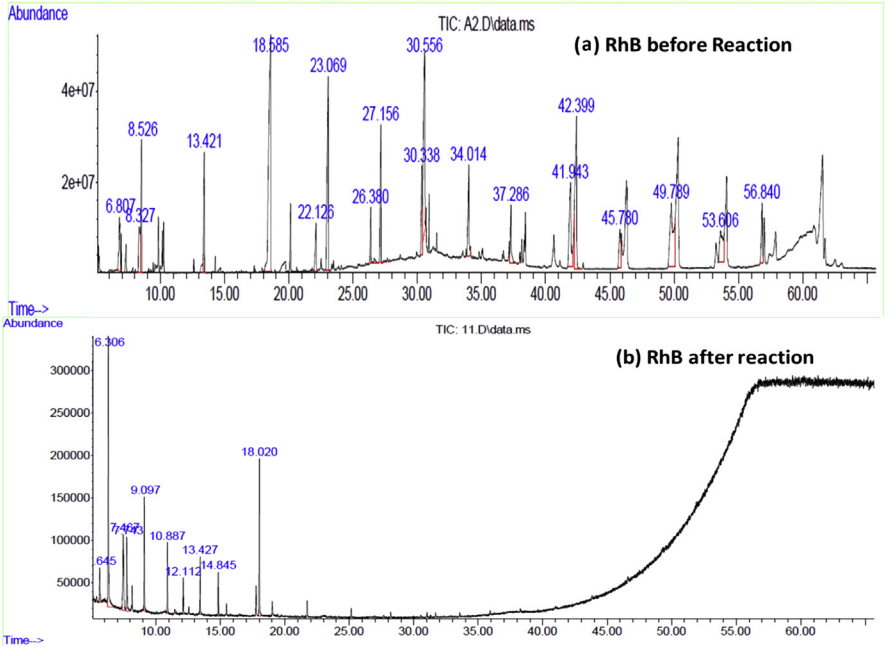

Fig. 14. GC-MS images of a) Initial concentration of RhB and b) After reaction take place in presence of Fe_3O_4-PVBC-PAC Au NPs catalysts.

5. Conclusion

In conclusion, the obtained K_{app} and TOF values for the degradation of RhBby Fe_3O_4-PVBC-g-PAC-AuNPs synthesized by SI-ATRP method showed an excellent catalytic activity as compared with suspension polymeric techniques methods. Among the different types Fe_3O_4-PVBC-g-PAC-AuNPs was found to be the best catalyst. TGA results of nano-composite catalyst showed 42 % of weight loss

https://doi.org/10.1016/j.heliyon.2018.e01005
2405-8440/© 2018 Published by Elsevier Ltd. This is an open access article under the CC BY-NC-ND license (http://creativecommons.org/licenses/by-nc-nd/4.0/).

compared with coated magnetic core-shell nanocomposites (60 % of weight loss). The TGA result reveals that the grafted polymerization is largely based on the core-shell polymerization. On the other hand, the saturation magnetisation of grafted core-shell is 16.50 emu/g. Besides, the recycling efficiency of magnetic core-shell catalyst viz, Fe_3O_4-PVBC-g-PAC-AuNPs were examined up to sixth cycle & no loss of catalytic activity were observed. The grafted magnetic core-shell Fe_3O_4-PVBC-g-PAC-AuNPs nanocomposites catalyst exhibited higher catalytic activity and reproducibility towards the degradation of RhB. Hence, the magnetic core-shell nanocomposite offers an excellent and environment friendly method for the removal of environmental pollutant RhB.

Declarations

Author contribution statement

A. Ramesh: Conceived and designed the experiments; Analyzed and interpreted the data; Wrote the paper.

P. Tamizhdurai, S. Gopinath, K. Sureshkumar: Performed the experiments; Analyzed and interpreted the data.

E. Murugan, K. Shanthi: Analyzed and interpreted the data; Contributed reagents, materials, analysis tools or data.

Funding statement

This research did not receive any specific grant from funding agencies in the public, commercial, or not-for-profit sectors.

Competing interest statement

The authors declare no conflict of interest.

Additional information

No additional information is available for this paper.

Acknowledgements

The authors gratefully acknowledge the financial supports for University Grants Commission (UGC), Defence Research and Development Organization (DRDO), Department of Science and Technology (DST) New Delhi. The author's also thankful to materials synthesis and characterization to provide the instruments facilities for Department of Physical Chemistry, University of Madras and Department of Chemistry, Anna University, Chennai to carry out this research work.

https://doi.org/10.1016/j.heliyon.2018.e01005
2405-8440/© 2018 Published by Elsevier Ltd. This is an open access article under the CC BY-NC-ND license (http://creativecommons.org/licenses/by-nc-nd/4.0/).

References

[1] H. Park, J. Park, A.K. Lim, E.H. Anderson, A.P. Alivisatos, P.L.M. Euen, Nano mechanical oscillations in a single-C60 transistor, Nature 47 (2000) 57−60.

[2] J. Gao, H. Gu, B. Xu, Multifunctional magnetic nanoparticles: design, synthesis, and biomedical applications, Acc. Chem. Res. 42 (2009) 1097−1107.

[3] L. Gao, J. Zhuang, L. Nie, J. Zhang, Y. Zhang, N. Gu, T. Wang, J. Feng, D. Yang, S. Perrett, X. Yan, Intrinsic peroxidase-like activity of ferromagnetic nanoparticles, Nat. Nanotechnol. 2 (2007) 577−583.

[4] Y.H. Deng, D.W. Qi, C.H. Deng, X.M. Zhang, D.Y. Zhao, Superparamagnetic high-magnetization microspheres with an Fe_3O_4@SiO_2 core and perpendicularly aligned mesoporous SiO_2 shell for removal of microcystins, J. Am. Chem. Soc. 130 (2008) 28.

[5] Z.C. Xu, Y.L. Hou, S.H.J. Sun, Magnetic core/shell Fe_3O_4/Au and Fe_3O_4/Au/Ag nanoparticles with tunable plasmonic properties, J. Am. Chem. Soc. 129 (2007) 8698−8699.

[6] C.T. Chen, Y.C. Chen, Fe_3O_4/TiO_2 core/shell nanoparticles as affinity probes for the analysis of phosphopeptides using TiO_2 surface-assisted laser desorption/ionization mass spectrometry, Anal. Chem. 78 (2005) 5912−5919.

[7] C.T. Chen, W.Y. Chen, P.J. Tsai, K.Y. Chien, J.S. Yu, Y.C. Chen, Rapid enrichment of phosphopeptides and phosphoproteins from complex samples using magnetic particles coated with alumina as the concentrating probes for MALDI MS analysis, J. Proteome Res. 6 (2007) 316−325.

[8] H.B. Na, I.C. Song, T.A. Hyeon, Inorganic nanoparticles for MRI contrast agents, Adv. Mater. 21 (2009) 2133−2148.

[9] H. Yu, M. Chen, P.M. Rice, S.X. Wang, R.L. White, S.H. Sun, Dumbbell-like bifunctional Au−Fe_3O_4 nanoparticles, Nano Lett. 5 (2005) 379−382.

[10] J.L. Hang, R.S. Srivastava, R.D.K. Misra, Core−shell magnetite nanoparticles surface encapsulated with smart stimuli-responsive polymer: synthesis, characterization, and LCST of viable drug-targeting delivery system, Langmuir 23 (2007) 6342−6351.

[11] M.H. Lee, J.L. Thomas, M.H. Ho, C. Yuan, H.Y. Lin, Antibiofouling polymer-coated superparamagnetic iron oxide nanoparticles as potential magnetic resonance contrast agents for in vivo cancer imaging, J. Am. Chem. Soc. 128 (2006) 7383−7389.

https://doi.org/10.1016/j.heliyon.2018.e01005
2405-8440/© 2018 Published by Elsevier Ltd. This is an open access article under the CC BY-NC-ND license (http://creativecommons.org/licenses/by-nc-nd/4.0/).

[12] Y. Zhu, L.P. Stubbs, F. Ho, R. Liu, C.P. Ship, J.A. Maruire, N.S. Hosmane, Magnetic nanocomposites: a new perspective in catalysis, Chem. Cat. Chem. 2 (2010) 365−374.

[13] J. Pyun, K. Matyjaszewski, Synthesis of nanocomposite organic/inorganic hybrid materials using controlled/"living" radical polymerization, Chem. Mater. 13 (2001) 3436−3648.

[14] T.V. Werne, T.E. Patten, Atom transfer radical polymerization from nanoparticles: a tool for the preparation of well-defined hybrid nanostructures and for understanding the chemistry of controlled/"living" radical polymerizations from surfaces, J. Am. Chem. Soc. 123 (2001) 7497−7505.

[15] K. Kamata, Y. Ln, Y.N. Xia, Synthesis and characterization of monodispersed core−shell spherical colloids with movable cores, J. Am. Chem. Soc. 125 (2003) 2384−2385.

[16] C.R. Vestal, Z.J. Zhang, Atom transfer radical polymerization synthesis and magnetic characterization of $MnFe_2O_4$/polystyrene core/shell nanoparticles, J. Am. Chem. Soc. 124 (2002) 14312−14313.

[17] K. Ohno, K. Koh, Y. Tsujii, T. Fukuda, Synthesis of gold nanoparticles coated with well-defined, high-density polymer brushes by surface-initiated living radical polymerization, Macromolecules 35 (2002) 8989−8993.

[18] Y. Shang, Z. Cao, H. Chen, Y. Sun, J. Yao, L. Yang, Influence of synthesis parameters on particle properties and catalytic activity of rice roll-like Au/SiO_2 nanocatalysts prepared in inverse miniemulsions, Colloids Surf. A 537 (2018).

[19] Y. Wang, X. Teng, J.S. Wang, H. Yang, Solvent-free atom transfer radical polymerization in the synthesis of Fe_2O_3@Polystyrene core−shell nanoparticles, Nano Lett. 3 (2003) 789−793.

[20] E. Cao, E. Prouzet, V. Héroguez, Harnessing the power of latex solutions based on titania particles − using si-ATRP towards larger surface modification for applications in gas separation membranes, Colloids Surf. A Physicochem. Eng. Aspects 510 (2016) 245−253.

[21] K. Fujimto, J.H. Kim, K. Ohmori, A. Ono, S. Shiratori, Flexible multilayer electrode films consisted of poly-aniline and polyelectrolyte by layer-by-layer self-assembly, Colloids Surf. A Physicochem. Eng. Aspects 313−314 (2008) 387−392.

[22] S.A. Nabavi, G.T. Vladisavljević, A. Wicaksono, S. Georgiadou, V. anović, Production of molecularly imprinted polymer particles with amide-decorated

https://doi.org/10.1016/j.heliyon.2018.e01005
2405-8440/© 2018 Published by Elsevier Ltd. This is an open access article under the CC BY-NC-ND license (http://creativecommons.org/licenses/by-nc-nd/4.0/).

cavities for CO_2 capture using membrane emulsification/suspension polymerization, Colloids Surf. A Physicochem. Eng. Aspects 521 (2017) 231−238.

[23] B. Lv, Z. Sun, J. Zhang, C. Jing, Multifunctional satellite Fe_3O_4-Au@TiO_2 nano-structure for SERS detection and photo-reduction of Cr(VI), Colloids Surf. A Physicochem. Eng. Aspects 513 (2017) 234−240.

[24] S. Kawada, D. Saeki, H. Matsuyama, Development of ultrafiltration membrane by stacking of silver nanoparticles stabilized with oppositely charged polyelectrolytes, Colloids Surf. A Physicochem. Eng. Aspects 451 (2014) 33−37.

[25] Q.L. Fan, K.G. Neoh, E.T. Kang, B. Shuter, S.C. Wang, Solvent-free atom transfer radical polymerization for the preparation of poly(poly(ethyleneglycol) monomethacrylate)-grafted Fe_3O_4 nanoparticles: synthesis, characterization and cellular uptake, Biomaterials 28 (2007) 5426−5436.

[26] L. Lei, X. Liu, Y.F. Li, Y.J. Cui, Y. Yang, G.R. Qin, Study on synthesis of poly(GMA)-grafted Fe_3O_4/SiO_X magnetic nanoparticles using atom transfer radical polymerization and their application for lipase immobilization, Mater. Chem. Phys. 125 (2011) 866−871.

[27] D. Radziuk, A. Skirtach, G. Sukhorukov, Stabilization of silver nanoparticles by polyelectrolytes and polyethylene glycol, Macromol. Rapid Commun. 28 (2007) 848−855.

[28] A. Stephen, K. Hashmi, G. Hutchings, Gold catalysis, J. Angew. Chem. 45 (2006) 7896.

[29] W.C. Ye, J.F. Yan, Q. Ye, F. Zhou, Template-free and direct electrochemical deposition of hierarchical dendritic gold microstructures: growth and their multiple applications, J. Phys. Chem. C 114 (2010) 15617−15624.

[30] Y. Li, E. Boone, M.E.I. Sayed, A size effects of PVP−Pd nanoparticles on the catalytic suzuki reactions in aqueous solution, Langmuir 18 (2002) 4921−4925.

[31] M. Zhao, L. Sun, R.M. Crooks, Preparation of Cu nanoclusters within Dendrimer templates, J. Am. Chem. Soc. 120 (1998) 4877−4878.

32 S. Gu, Y. Lu, J. Kaiser, M. Albrecht, M. Ballauf, Kinetic analysis of the reduction of 4-nitrophenol catalyzed by Au/Pd nanoalloys immobilized in spherical polyelectrolyte brushes, Phys. Chem. Chem. Phys. 17 (2015) 28137−28143.

https://doi.org/10.1016/j.heliyon.2018.e01005
2405-8440/© 2018 Published by Elsevier Ltd. This is an open access article under the CC BY-NC-ND license (http://creativecommons.org/licenses/by-nc-nd/4.0/).

[33] A. Roucoux, J. Schulz, H. Patin, Reduced transition metal colloids: a novel family of reusable catalysts, Chem. Rev. 102 (2002) 3757−3778.

[34] R.M.C. Zhao, M.L. Sun, V. Chechik, L.K. Yeung, Dendrimer-encapsulated metal nanoparticles: synthesis, characterization, and applications to catalysis, Acc. Chem. Res. 34 (2001) 181−190.

[35] A. Lunhong, Z. Chunmei, W. Qinmin, One-step solvothermal synthesis of Ag-Fe_3O_4 composite as a magnetically recyclable catalyst for reduction of Rhodamine B, Cat. Commun. 14 (2011) 68−73.

[36] D. Astruc, F. Lu, J.R. Aranzaes, Nanoparticles as recyclable catalysts: the frontier between homogeneous and heterogeneous catalysis, Angew. Chem. Int. Ed. 44 (2005) 7852−7872.

[37] W. Yao, B. Zhang, C. Huang, C. Ma, X. Songa, Q. Xu, Synthesis and characterization of high efficiency and stable Ag_3PO_4/TiO_2 visible light photocatalyst for the degradation of methylene blue and rhodamine B solutions, J. Mater. Chem. 22 (2012) 4050−4055.

[38] K. Santhy, P. Selvapathy, Removal of reactive dyes from wastewater by adsorption on coir pith activated carbon, Bioresour. Tech. 97 (2006) 1329−1336.

[39] G. Mckay, M.S. Otterburn, D.A. Aga, Evaluation of fly ash as an adsorbent for the removal of methylene blue from its aqueous solution, Water Air Soil Pollut. 24 (1985) 307.

[40] P. Shamsh, G. Panday, D.A. Aga, Orange peel as an adsorbent in the removal of acid orange 17(acid dye) from aqueous solution, Ind. J. Environ. Health 36 (1994) 263.

[41] M. Sarioglu, U. Atay, Removal of methylene blue by using bio solid, Global Nest. J. 8 (2006) 113−120.

[42] W.M. Daoush, Co-precipitation and magnetic properties of magnetite nanoparticles for potential biomedical applications, J. Nanomed. Res. 5 (2017) 1−6.

[43] M. Masoud, Recent advances in catalysts immobilized on magnetic nanoparticlesJ, Iran Chem. Soc. 13 (2016) 1827−1845.

https://doi.org/10.1016/j.heliyon.2018.e01005
2405-8440/© 2018 Published by Elsevier Ltd. This is an open access article under the CC BY-NC-ND license (http://creativecommons.org/licenses/by-nc-nd/4.0/).